Hindawi Publishing Corporation
Shock and Vibration
Volume 2014, Article ID 432760, 15 pages
http://dx.doi.org/10.1155/2014/432760

Research Article

Excellent Performance of Earth Dams under Resonance Motion Using Isolator Damping Layer

Behrouz Gordan and Azlan Adnan

Engineering Seismology and Earthquake Engineering Research Group (e-SEER), Universiti Teknologi Malaysia, 81310 Skudai, Johor, Malaysia

Correspondence should be addressed to Azlan Adnan; azlanadnan@utm.my

Received 20 February 2014; Accepted 22 April 2014; Published 22 May 2014

Academic Editor: Alicia Gonzalez-Buelga

The effect of blanket layer using isolator damping layer (IDL) between river sand foundation and short embankment to remove damage under severe earthquake was investigated in the present study. In case of numerical analysis by ANSYS program, dominant frequency (DF) was computed by free vibration analysis. Soil mechanic tests for thirteen samples to design IDL formula were carried out. In terms of critical condition for earthquake effect such as resonance, five physical small models were tested using vibrator table under the dominant frequency with scale parameter 1/100. As a result, dam was significantly damaged without blanket layer IDL. In order to reduce damage, the best performance was observed using blanket layer (IDL) when this layer was expanded below the reservoir region. The reinforced thickness layer size is one-fourth of dam height. This method is a novel suggestion for earth dam design in seismic zone.

1. Introduction

The dynamic assessment dramatically has been started in earth dams after the observation of some damages during the earthquake. In this domain, huge damage such as body cracks was recorded. Totally, this knowledge is correspondent to control dam behavior to avoid of failure process. Besides, earth dam construction is possible with respect to compaction process. Therefore, the consolidation settlement can be completely maximized at the end of construction. In terms of earthquake effect on dam response, the first phase of total settlement is related to the final displacement in the static state. Therefore, total settlement is the superposition of static and dynamic effect. According to literature review in this study, a few cases of data monitoring was just recorded [1–3]. Two cases such as the lack of data monitoring and technological development to provide computing program led to use of numeric method for dynamic analyzing. In the other words, the numerical analysis was commonly utilized in several studies to predict dynamic behavior during the earthquake [4–9]. In terms of analysis technique, two methods such as finite-element method (FEM) and finite-difference method (FDM) can be applied. Dynamic analysis of earth dam was carried out by using two techniques such as two-dimensional and three-dimensional [10–13]. To select, plane strain (2D) and plane stress (3D) depends on dam configuration and valley shape in order to distribute lateral strain [14]. In terms of reinforcement methods, some methods have been used to reinforce dam in order to improve dynamic behavior along the earthquake [15–19]. To verify results based on numeric analysis, both tests such as shaking table and centrifuge were successfully experienced [20–22]. However, to avoid dam failure by earthquake, the effect of foundation soil was of a significant role to generate cracks with respect to increase of acceleration and displacement at the crest. In the present study, the main purpose is the improvement of dam performance under severe motion like resonance condition using blanket layer between foundation and homogenized earth dam. In other words, this paper presents a novel method to remove damage by using new material (IDL). In order to discuss level of damage in dam, five physical models in regard to dominant frequency will

be vibrated. To improve dam performance, the optimum thickness will be finally suggested.

2. Laboratory Soil Tests

Two types of experimental tests were carried out in this study. Firstly, soil mechanic tests were performed based on British Standard (BS) in order to design isolator damping layer (IDL). Secondly, some small scale models with respect to finding the best location to reinforce dam were vibrated by using vibrator table. In terms of soil characters, the British Standard (BS) for soil mechanic tests was used. Based on soil classification, the local laterite soil MH was applied. The summarizing of laterite properties is illustrated in Table 1, as used in this study.

The passing percentage for different materials such as laterite, tire derived aggregate (TDA), and microsilica (MS) was shown in Figure 1. The determination of particle size distribution was carried out by using BS 1377-2 1990. This figure shows that the amplitude of material size was located between 0.075 mm and 2.00 mm. Based on specific gravity test, this value for MS was more than TDA. These values were, respectively, exposed at 2.42 and 2.15. Table 2 shows samples with respect to different mixtures to design IDL.

According to soil laboratory test, undrained shear strength in the triaxial compression without measurement of pore pressure (quick undrained) indicated that the strain in samples is increased by using more percentage of TDA; it can be observed in Figure 2. Also in this figure, elasticity modulus is reduced (see histograms in Figure 3). Significantly, the yield point was dramatically reduced in this trend. With respect to increasing flexibility by using maximum TDA, failure stress is possible with lower value. Figure 3 shows that the increase of TDA has effectively led to decrease of elasticity modulus that was obtained with 90.21% for sample 5. In fact, the elasticity modulus was significantly decreased by using 10% TDA, as mentioned previously. Moreover, the maximum and minimum values of modulus elasticity were, respectively, obtained in sample 1 and sample 5, as can be seen in Figure 4. It is worth noting that the regular increase of the modulus was just found in sample 4 by increase of microsilica with 7% of TDA (see Figure 5, histogram without filling). In terms of flexibility distribution in samples, the maximum and minimum value of the area below curve were located in sample 8 and sample 5, as shown in Figure 6. In addition, the good convergence for sample 9 and sample 1 was obtained. It should be noted that the quick undrained results were computed by average from three cases. After all, flexibility factor has the important role in order to absorb energy.

According to consolidation test, the maximum coefficient of volume compressibility was located in sample 6 with 0.207 while the minimum value was in sample 13 with 0.081 (see Figure 7(a)). It was revealed that the increase of TDA for samples 1 to 5 caused increasing of rate regardless of sample 2. In fact, this coefficient was double value for sample 5 with 10% TDA. In addition, the minimum value was observed by 10% TDA with 4% silica (see sample 12). Also in Figure 7(b), the maximum and minimum coefficient of consolidation were, respectively, observed in sample 6 and sample 10. This factor was progressively reduced by more percentage of TDA and silica. Therefore, the impact of silica to decrease consolidation coefficient was greater than TDA.

It should be noted that the determination of the one-dimensional consolidation properties based on BS 1377-5 1990 was carried out. All samples were tested by using loads such as 25, 50, 99.9, 199.80, 399.70, and 799.4 Kilo Pascal. In addition, in order to evaluate unloading effect to compute compression index, the load of samples was declined with regard to 399.70, 199.80, and 99.90 Kilo Pascal. In this test, the test duration for each sample was nine days. Moreover, the logarithmic-time method was used to identify void ratio distribution with respect to applied pressure. Consequently, both coefficients as discussed were computed by average value based on different pressure with respect to loading stages.

In terms of permeability assessment, sample 5 shows the maximum permeability regarding use of 10%TDA (see

Table 1: Characteristics of the laterite soil.

Physical properties	Value
Specific gravity	2.40
Liquid limit, LL (%)	75
Plastic limit, PL (%)	41
Plasticity index, PI (%)	34
BS classification	MH
Maximum dry density ($g\,cm^{-3}$)	1.33
Optimum moisture content (%)	35
Unconfined compressive strength (KPa)	306.26
Cohesion (KPa)	25.18
Angle of internal friction (degree)	30.00
Modulus elasticity (KPa)	15283.72
Coefficient of volume compressibility (mv, m^2/MN)	0.1055
Coefficient of consolidation (cv, m^2/yr)	44.16
Permeability (cm/seconds)	$1.29E-5$

Table 2: Sample definition.

Sample number	Component
1	Laterite
2	Laterite + 3% TDA
3	Laterite + 5% TDA
4	Laterite + 7% TDA
5	Laterite + 10% TDA
6	Laterite + 3% TDA + 2% silica
7	Laterite + 3% TDA + 3% silica
8	Laterite + 5% TDA + 2% silica
9	Laterite + 5% TDA + 3% silica
10	Laterite + 7% TDA + 3% silica
11	Laterite + 7% TDA + 4% silica
12	Laterite + 10% TDA + 4% silica
13	Laterite + 10% TDA + 5% silica

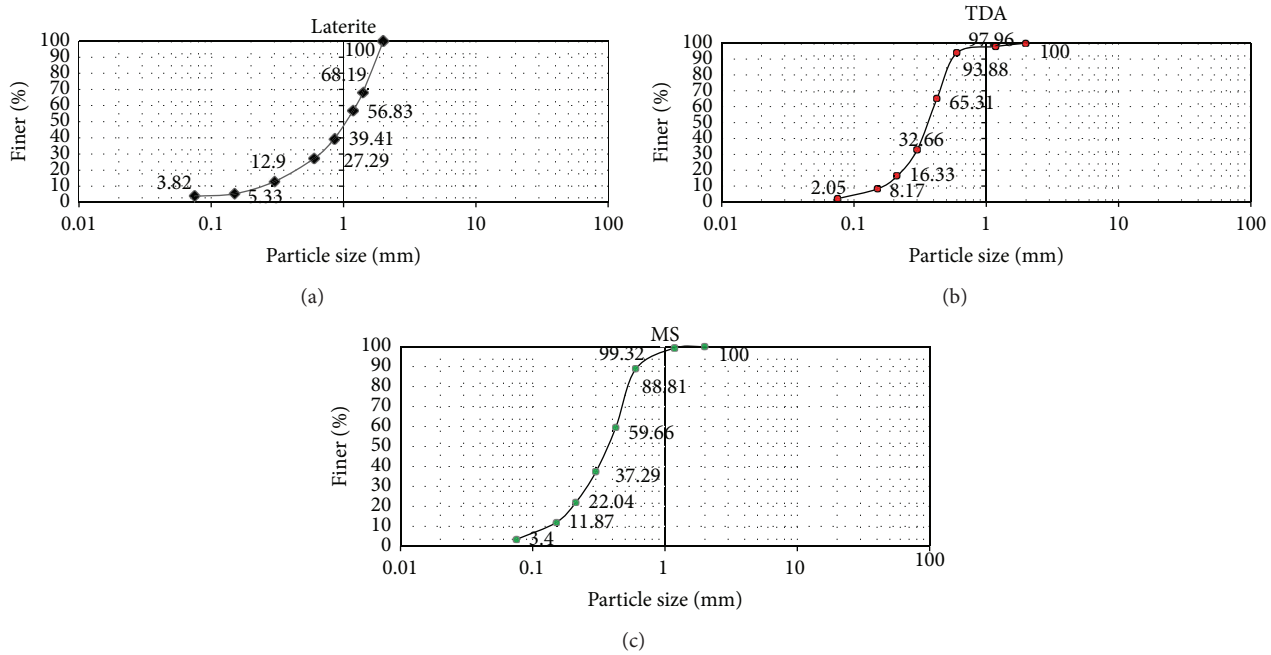

Figure 1: Distribution of gradation for different materials. (a) Laterite, (b) tire driven aggregate, and (c) microsilica.

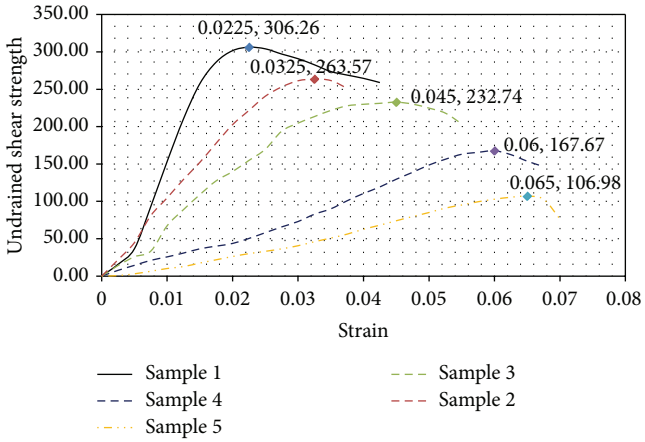

Figure 2: Undrained shear strength in the triaxial compression without measurement of pore pressure, sample 1 to sample 5.

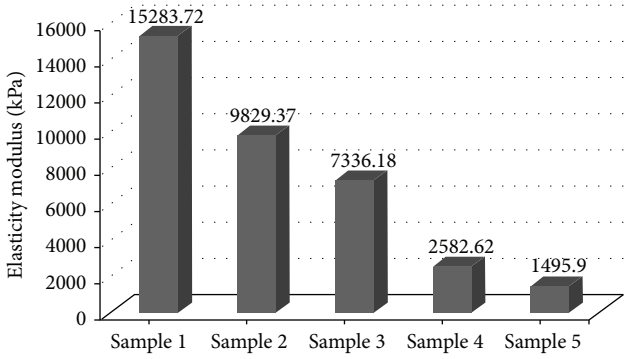

Figure 3: Distribution of elasticity modulus in samples one to five.

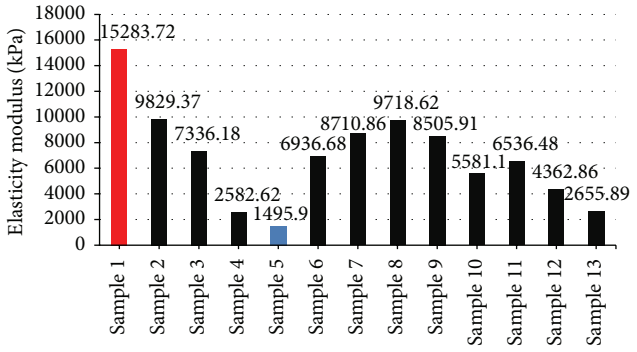

Figure 4: Distribution of elasticity modulus in samples.

Figure 8). However, one of the major factors to design dam is seepage controlling. Therefore, the permeability index was significantly improved by using more percentage of silica in this study. In Figure 8, the minimum permeability was observed in sample 10 ($1.67E-5$ cm/s).

In terms of shear strength assessment using direct shear test (small shear box apparatus), sample 10 indicated the best performance in order to increase both factors of cohesion and internal angle of friction. Table 3 shows distribution of cohesion and internal angle of friction in different samples.

In order to estimate the damping ratio, the nonlinear stress-strain characteristics of soils (Figure 9(a)), for analysis purposes, can be represented by bilinear relationships (Figure 9(b)) or multilinear relationships. However, the use of an equivalent linear viscoelastic analysis leads to similar results. Damping ratio depends on both areas as can be seen

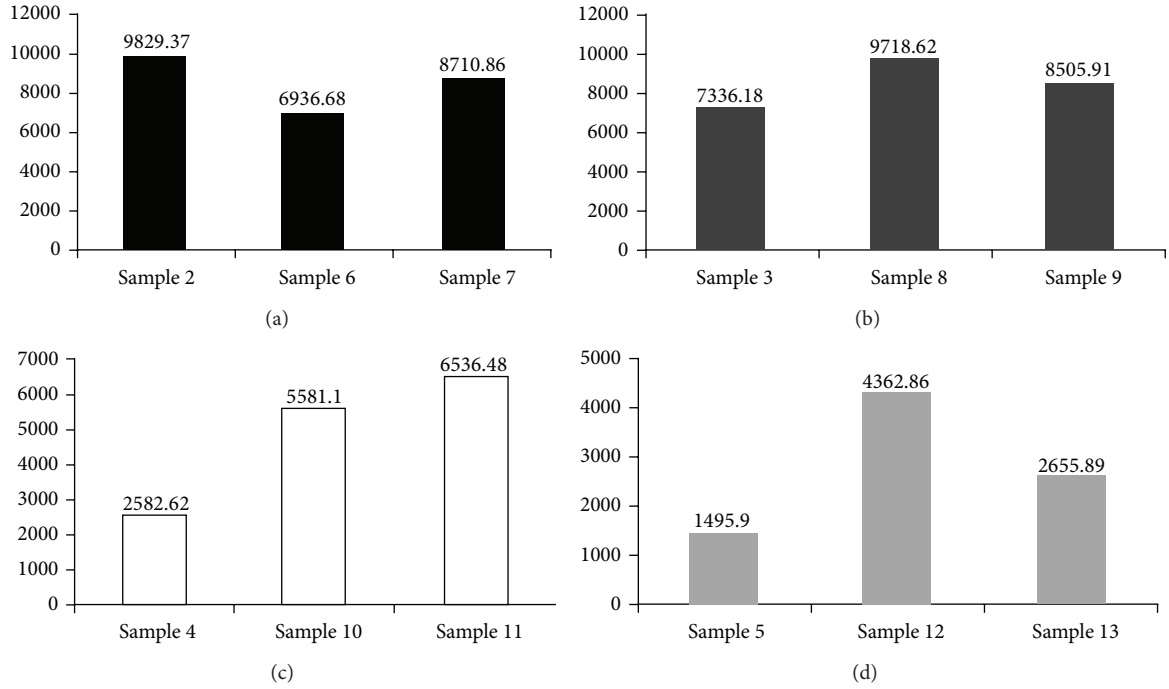

Figure 5: Distribution of elasticity modulus (Kilo Pascal) for samples.

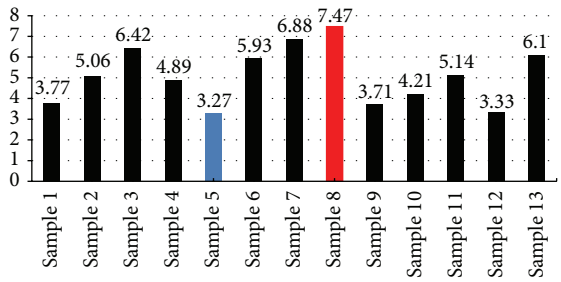

Figure 6: Distribution of area under the curve of stress-strain based on unconfined test.

with blue and red colors in this figure [24]. This ratio can be given as follows:

$$\text{Damping ratio} = D = \left(\frac{1}{4\pi}\right) * \left(\frac{\text{Loop area}}{\text{area under stress strain curve}}\right). \quad (1)$$

However, the area under stress strain curve and hysteresis loop area can be computed according to Figure 9. Figure 10 shows damping ratio for sample 1 and sample 10, respectively. It can be seen that this ratio was 17.95% in laterite soil. In terms of soil improvement, the damping coefficient increased to 22.63% for sample 10 (7% TDA with 3% silica).

After discussing all tests in soil mechanic that were carried out, sample 10 shows the excellent performance in order to reinforce dam. Therefore, IDL material was defined by using sample 10. In the physical small dam modeling, this material to reinforce dam in different location was used.

For small scale modeling, the river sand was used for foundation. Table 4 presents sand properties. It is important to note that river sand included uniform size particles because uniformity coefficient was less than five. In addition, coefficient of curvature was less than one. The soil is said to be well graded if this value lies between one and three. Therefore, this type of sand was selected in order to critically condition foundation.

Table 3: Distribution of cohesion and angle of internal friction in different samples.

Sample	Cohesion (KPa)	Friction (degree)
1	25.18	30.00
2	13.17	35.01
3	22.34	31.07
4	13.05	36.33
5	30.1	29.39
6	14.74	33.6
7	16.82	33.58
8	18.15	33.47
9	15.57	36.31
10	26.38	32.10
11	34.94	28.57
12	27.11	28.67
13	14.86	32.52

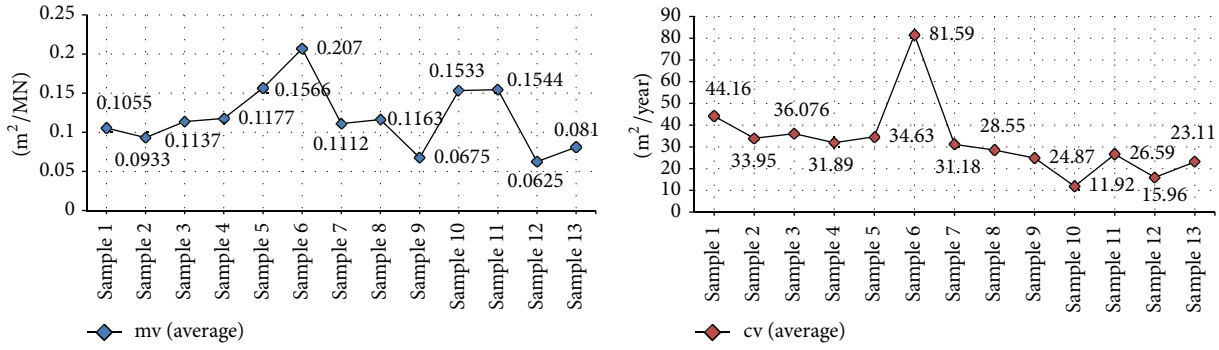

(a) Coefficient of volume compressibility

(b) Coefficient of consolidation

Figure 7: Distribution of coefficients in samples for consolidation test. (a) Coefficient of volume compressibility and (b) coefficient of consolidation.

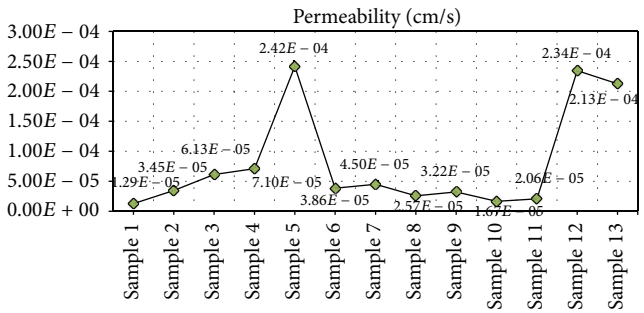

Figure 8: Distribution of permeability for different samples.

Table 4: Sand properties.

Physical properties	Value
Specific gravity	2.547
Cohesion (KPa)	0.00
Angle of internal friction (Degree)	35
Modulus elasticity (KPa)	32460
Maximum dry density (gr/cm^3)	1.72
Minimum dry density (gr/cm^3)	1.36
Density for I_d = 75% (gr/cm^3)	1.613
Permeability (cm/s)	0.1
Maximum size (mm)	2.00
Minimum size (mm)	0.075
Uniformity coefficient C_u	4.375
Coefficient of curvature C_c	0.97

3. Small Scale Model on Vibrator Table

Physical models with scale parameter equal to 1/100 were tested. In order to research methodology for this purpose, some aspects included characteristic of vibrator table, displacement transducer, data logger, sinusoidal motion, scale parameter for static or dynamic condition, free vibration analysis, and physical modeling will be presented. In this study, five small scale dams were tested, as will be explained in the next section.

3.1. Vibrator Table. In this study, vibrating table 24-9112 (CN-166) with respect to sinus motion was used. Figure 11 shows the vibrating desk that was cushioned with steel and seminoiseless electromagnetic vibrator with 3600 vpm operating frequency. In addition, it has a separate controller to vary vibrator amplitude in case of frequency capacity limit 100 Hz. Table capacity was equal to 750 lbs (340 kg). Double amplitude range was located at 0.002 inch (0.05 mm) to 0.015 inch (0.38 mm). Actuator was an electromagnetic vibrator over 100 lbs (45.30 kg). The table was square in shape and 30 inch (762 mm). The table thickness was 33.3 mm of steel. In case of weight, it was net 555 lbs (252 kg) and shipping was 605 lbs (274 kg). Figure 11 illustrates the vibrator table for this study.

3.2. Displacement Transducerand Data Logger. Displacement transducer CDP-D was utilized with respect to dual isolated I/O ports. By using transducer, one set of cables for input and output was connected to the analog measuring instrument and another set to the digital measuring instrument. With two different types of measuring equipment connected to this transducer, simultaneous measurements can be made without interference. Figure 12(a) shows the displacement transducer and Figure 12(b) shows the dimensions for transducer CDP-100. To measure displacement at both edges of the crest in small scale modeling, two transducers were installed. In terms of data record, data logger or data recorder is an electronic device that records data over time or in relation to location with either a built in instrument or a sensor or via external instruments and sensors.

Figure 12(c) illustrates the data logger that was used in this study. Based on device ability, results were printed during the vibration duration. After that, results were classified by using Excel program. It should be noted that both transducers as mentioned previously were connected to this data logger (UCAM-70A) in order to record vertical displacement during the vibration. In addition, the sub step of vibration period was

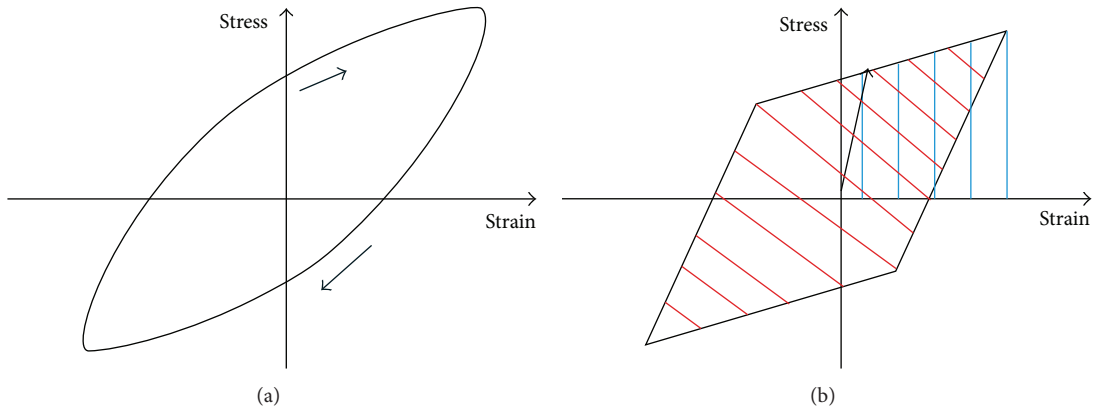

Figure 9: Damping definition and hysteretic and equivalent bilinear stress-strain relationships for soil: (a) stress-strain curves; (b) bilinear idealization [23].

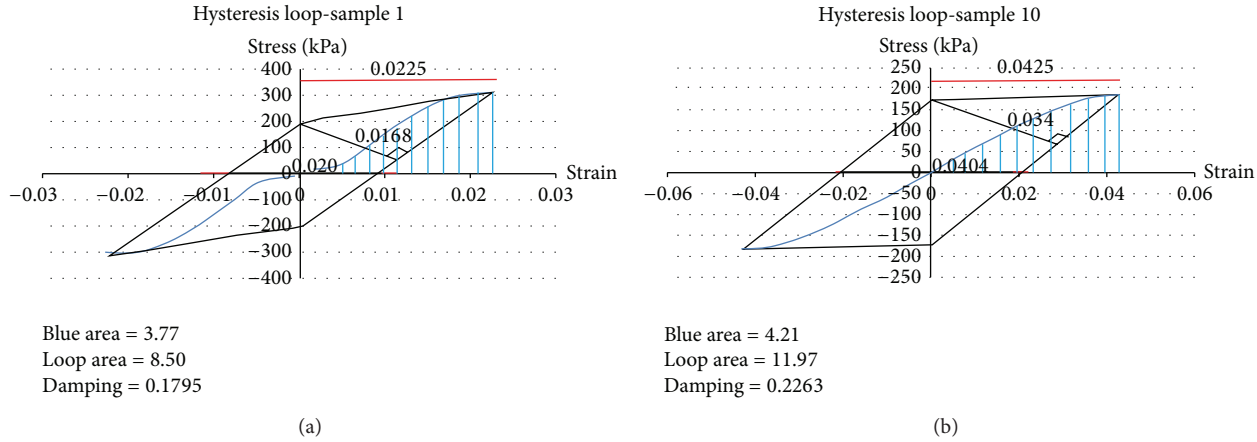

Figure 10: Estimation of damping ratio: (a) sample 1 and (b) sample 10.

Figure 11: Vibrator table.

Table 5: Conversion for peak value in sinusoidal motion, displacement (X), velocity (V), acceleration (A), and frequency (f).

	Displacement, X	Velocity, V	Acceleration, A
Displacement, X	$X = X$	$X = \frac{V}{2\pi f}$	$X = \frac{A}{(2\pi f)^2}$
Velocity, V	$V = 2\pi f X$	$V = V$	$V = \frac{A}{2\pi f}$
Acceleration, A	$A = (2\pi f)^2 X$	$A = 2\pi f V$	$A = A$

equal to two seconds based on device ability with respect to print.

3.3. Sinusoidal Vibrate Loading. There is a mathematical relationship between frequency, displacement, velocity, and acceleration for sinusoidal motion according to consideration of the peak value for them. The relationship is such that if any two of the four variables are known, the other two can be calculated. Table 5 shows all equations that were provided in this context [25].

G in these formulas is not gravity acceleration. It is a constant for calculation within different systems. Respectively, for metric, imperial, and Si, G is 9.80665 m/s^2, 386.0885827 in/s^2, and 1.00 m/s^2.

Since the motion is sinusoidal, the displacement, velocity, and acceleration are changing sinusoidal trend. However, they are not in the same phase. The phase relationship between displacement, velocity, and acceleration is that velocity is 90° out of phase with acceleration and displacement is 180° out of phase with acceleration.

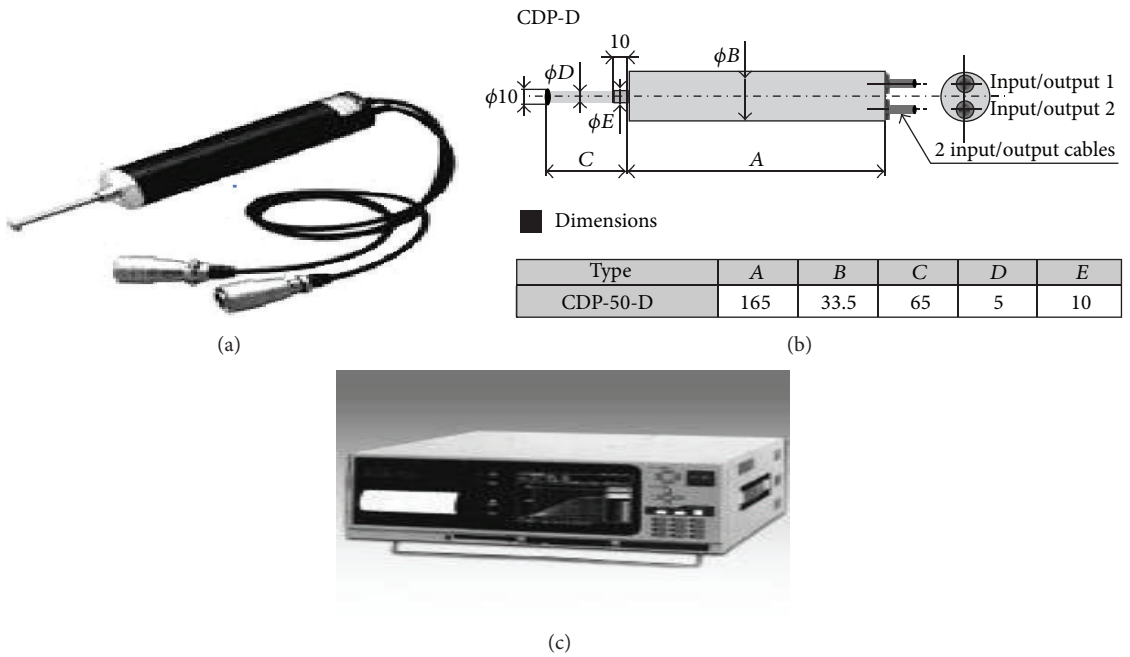

Type	A	B	C	D	E
CDP-50-D	165	33.5	65	5	10

FIGURE 12: Transducer and data logger. (a) Displacement transducer, CDP-100, (b) dimension of displacement transducer (CDP-100), and (c) data logger, UCAM-70A.

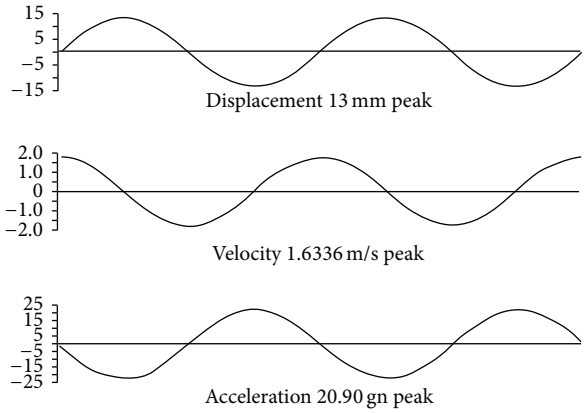

FIGURE 13: 20 Hz sinusoidal motion.

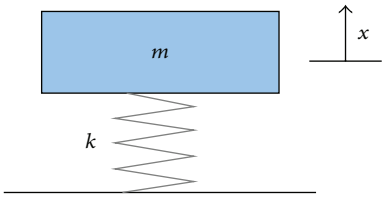

FIGURE 14: Mass spring system.

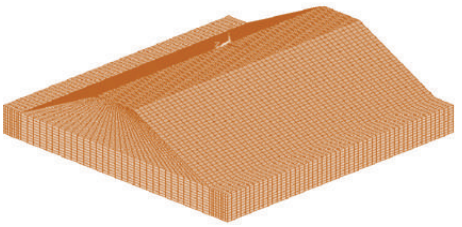

FIGURE 15: Free mesh.

In other words, when displacement is at a maximum, velocity is at a minimum, and acceleration is at a maximum. It should be noted that 1 g_n = 9.80665 m/s^2 = 32.174 ft/s^2 = 386.0886 in/s^2. Figure 13 shows the example of displacement distribution with velocity and acceleration while the frequency of sinusoidal motion is twenty hertz.

3.4. Scaling Laws. In case of the scale parameter, the scale factor can be used according to

$$x^* = \frac{x_m}{x_p}. \tag{2}$$

The subscript m represents "model" and the subscript p represents "prototype" and x^* represents the scale factor for the quantity x [26].

The reason for spinning a model on a centrifuge is to enable small scale models to feel the same effective stresses as a full scale prototype. This goal can be stated mathematically as

$$\sigma'^{x} = \frac{\sigma'_m}{\sigma'_p} = 1, \tag{3}$$

where the asterisk represents the scaling factor for the quantity, σ'_m is the effective stress in the model, and σ'_p is the effective stress in the prototype.

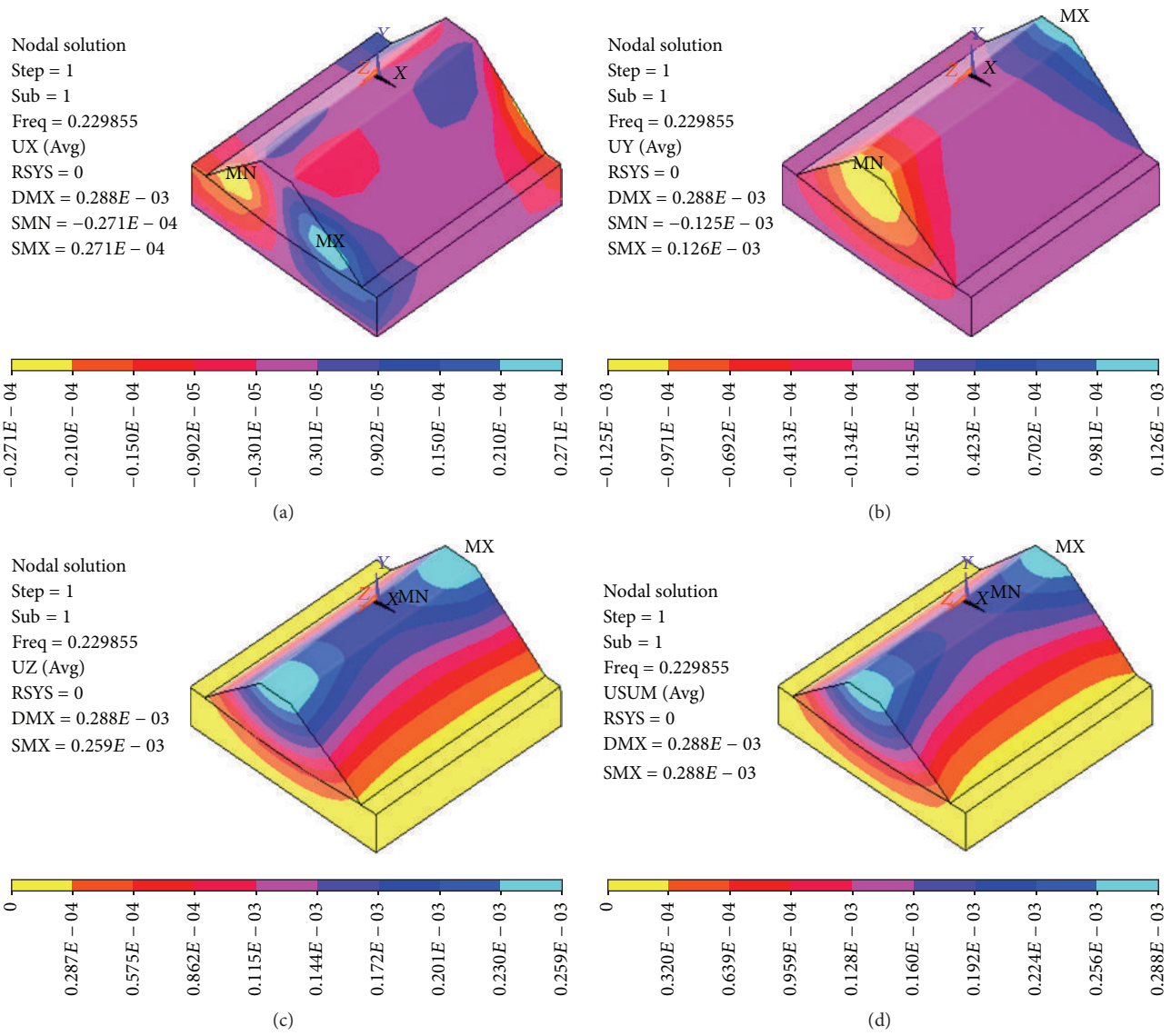

Figure 16: Mode shape 1. (a) horizontal displacement, (b) vertical displacement, (c) lateral displacement, and (d) total displacement.

In soil mechanics, the vertical effective stress, σ', for example, is typically calculated by

$$\sigma' = \sigma^t - u, \tag{4}$$

where σ^t and u are total stress and pore pressure, respectively. For a uniform layer with no pore pressure, the total vertical stress at a depth H may be calculated by

$$\sigma^t = \rho g H, \tag{5}$$

where ρ represents the density of the layer and g represents gravity. In the conventional form of centrifuge modeling [26], it is typical that the same materials are used in the model and prototype; therefore, the densities are the same in model and prototype; that is,

$$\rho^* = 1. \tag{6}$$

Furthermore, in conventional centrifuge modeling all lengths are scaled by the same factor L^*. To produce the same stress in the model as in the prototype, we thus require

$$\rho^* g^* H^* = 1 g^* L^* = 1. \tag{7}$$

It may be rewritten as

$$g^* = \frac{1}{L^*}. \tag{8}$$

The above scaling law states that if lengths in the model are reduced by some factor, n, then gravitational accelerations must be increased by the same factor, n, in order to preserve equal stresses in model and prototype.

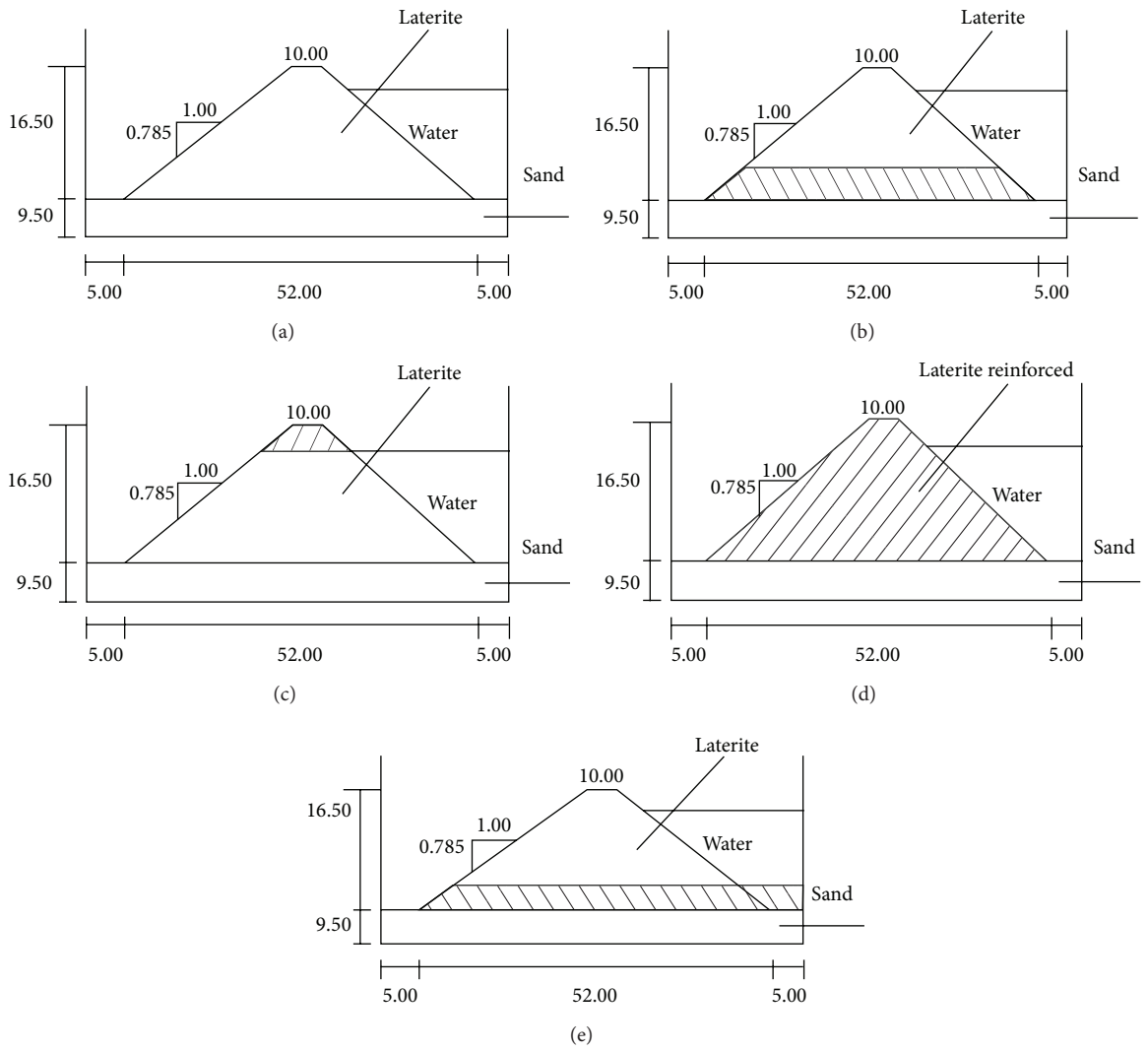

Figure 17: Model introducing ((a), (b), (c), (d) and (e)) for small dam (cm) ($S = 1/100$).

For dynamic problems where gravity and accelerations are important, all accelerations must scale as gravity is scaled; that is,

$$a^* = g^* = \frac{1}{L^*}. \tag{9}$$

Since acceleration has units of L/T^2, it is required that

$$a^* = \frac{L^*}{T^2}. \tag{10}$$

Hence, it is required that

$$\frac{1}{L^*} = \frac{L^*}{T^2}, \quad \text{or} \quad T^* = L^*. \tag{11}$$

Frequency has units of inverse of time and velocity has units of length per time, so for dynamic problems we also obtain

$$f^* = \frac{1}{L^*}, \qquad v^* = \frac{L^*}{T^*} = 1. \tag{12}$$

For model tests involving dynamics, the conflict in time scale factors may be resolved by scaling the permeability of the soil [26].

3.5. Free Vibration Analysis. In dynamic assessment, free vibration analysis is the base of study. In fact, the distribution of frequency in the different vibration mode can be computed by the application of modal analysis based on finite-element method (FEM). It is worth mentioning that, this analysis is perfectly related to the mass and spring. In case of the mass-spring-damper system, the first assumption is negligible about damping effect. Therefore, there is not any external force on mass in this state. The force applied to the mass by the spring is proportional to the amount of the spring that is stretched "x" (it can be assumed that spring is already compressed due to the weight of the mass). The proportionality constant (k) is spring stiffness (see Figure 14). The unit measurement is force divided by distance (kg/m).

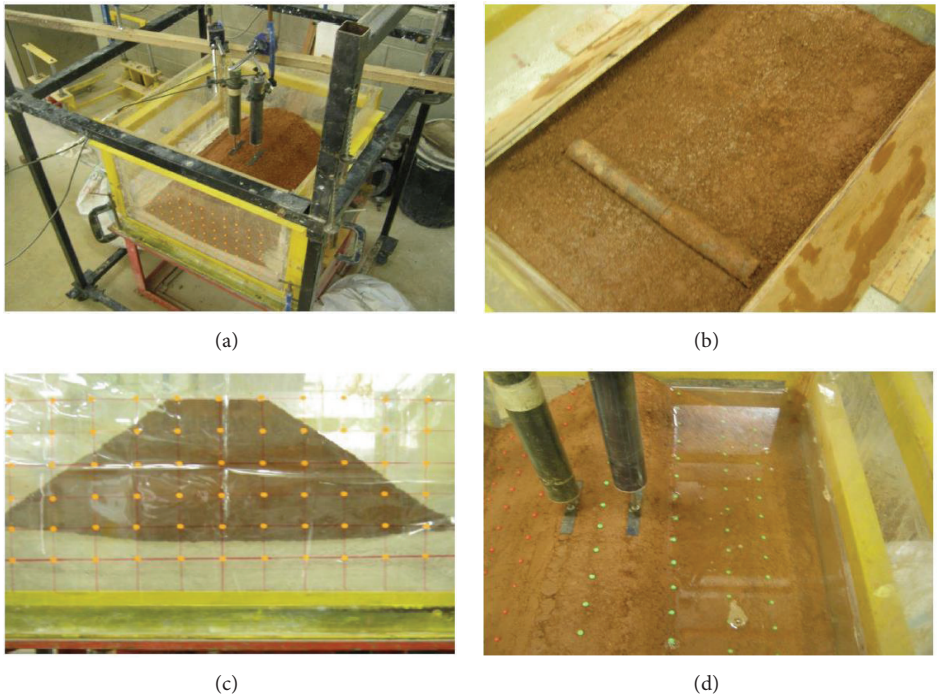

(a) (b) (c) (d)

Figure 18: Small scale dam. (a) Dam perspective with two LVDT, (b) soil compaction with roller, (c) dam section with index network, and (d) dam with tank before vibration.

The negative sign indicates that force is always opposing the motion of the mass attached to it according to the following equation:

$$F_s = -kx. \tag{13}$$

The force generated by the mass is proportional to the acceleration of the mass as given by Newton's second law of motion

$$\sum F = ma = m\ddot{x} = m\frac{d^2x}{dt^2}. \tag{14}$$

The sum of the forces on the mass then generates this ordinary differential equation

$$m\ddot{x} + kx = 0. \tag{15}$$

Assuming that the initial vibration can be started by stretching and releasing the spring with distance (A), the solution to the above equation that describes the motion of mass can be seen in the following equation:

$$x(t) = A\cos\left(2\pi f_n t\right). \tag{16}$$

This solution shows that it will oscillate with simple harmonic motion that has amplitude of (A) and a frequency (f_n). The number (f_n) is called the undamped natural frequency. For the simple mass-spring system, frequency is given by

$$f_n = \frac{1}{2\pi}\sqrt{\frac{k}{m}}. \tag{17}$$

However, the relation between frequency and vibration period is always reverse. Consider

$$T = \frac{1}{f}. \tag{18}$$

In terms of the measurement unit, the vibration period and frequency were according to seconds and hertz. It is worth noting that the dominant frequency is the minimum frequency to produce maximum vibration period.

4. Numerical Analysis

In terms of numerical analysis, modal analysis was carried out by using ANSYS program in this study to compute dominant frequency for small scale model regarding 3D analysis. This program is one of the famous software programs with respect to finite-element method (FEM). In particular, this software is one of the universal programs with high level of the ability for different analyses. A strong ability to compute free vibration analysis is possible with modal analysis [27].

4.1. Elements and Meshing Process. To select element based on Help menu, solid 8 nodes 183 (3D) were used for this purpose. Figure 15 shows the mapped mesh for numerical modeling. In this figure, 23956 elements and 35457 nodes in models were used for free vibration analysis. According to this condition, free vibration analysis to access frequency in different vibration modes was carried out, as results can be discussed in the next section.

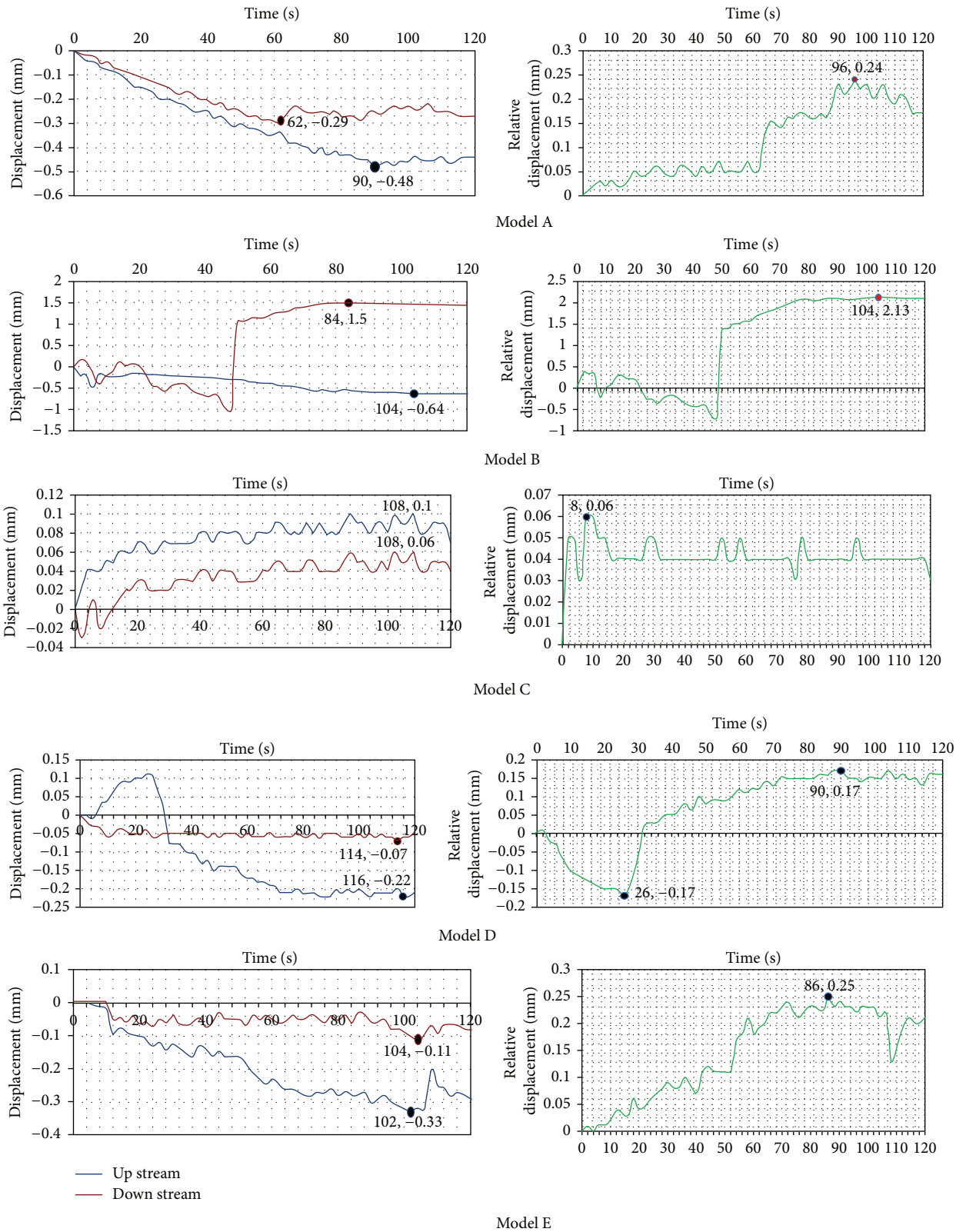

Figure 19: Vertical displacement in both edges of the crest in models with relative displacement.

(a) (b) (c)

Figure 20: Damage in the first model (Model A).

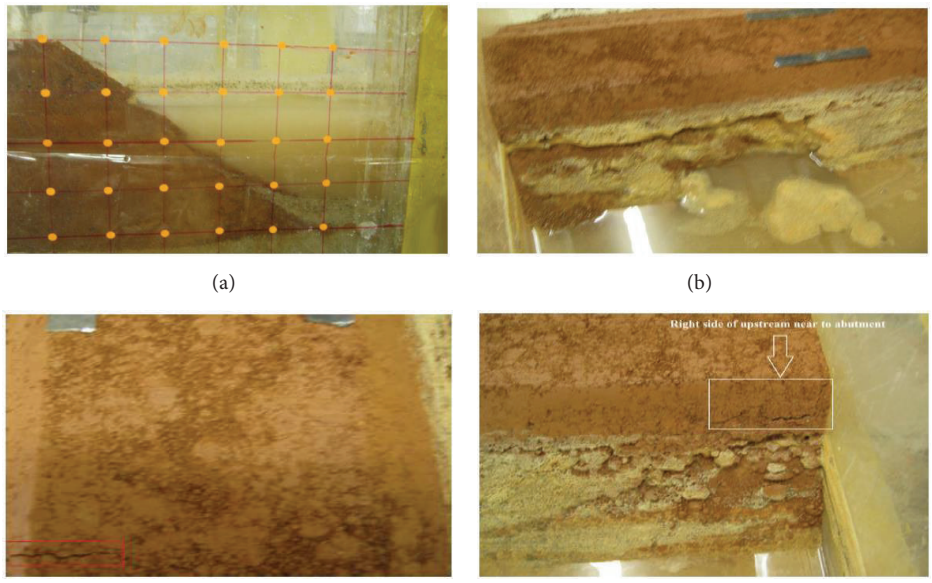

(a) (b)

(c) (d)

Figure 21: Damage in the second model (Model B).

4.2. Free Vibration Analysis and Dominant Frequency. In terms of modal analysis, the free vibration analysis was calculated by ANSYS program. Figure 16 shows displacement in three directions of model and total displacement in the first vibration mode, because, based on distribution of frequency in the first mode to fifth mode, it is important to note that the minimum frequency (0.22986 Hz) was observed in the first vibration mode. It means that the vibration period was maximum and critical in this mode.

Distribution of frequency in different vibration modes indicated that this value was, respectively, obtained at 0.26257 Hz, 0.28387 Hz and 0.30135 Hz in the vibration shape modes 2 to 4.

5. Results and Discussion Based on Physical Small Scale Modeling

In order to find the best location of reinforcement in dam, five small dams with different locations of reinforcement using IDL material were vibrated by dominant frequency (22.986 Hz) with respect to resonance condition. Figure 17 shows five small scale dams (Models (a), (b), (c), and (d)); it is obvious that models have the same dimension. In this figure, the reinforced area was illustrated with a hatch area. For example, Model (d) indicated that all dam body was reinforced. For this purpose, one steel box for modeling was used. This box made by five sheets of Plexiglas with 20 mm thickness. One of them was in the base of model. The level of reservoir was 75% of the dam height. The scale parameter was 1/100. It means that model was one hundred times smaller than prototype. The dam height was 22.7 meter in reality but it was made 22.7 cm in physical model. In addition, small scale modeling was coupled by foundation. Foundation material was dense sand with 75% relative density. Sand properties were mentioned in soil mechanic test. Figure 18 shows some details including dam perspective, soil compaction, network index, and reservoir. In this Figure, two LVDT on the middle of model at the both edges of the crest were installed. In order to achieve support, one steel frame and one steel beam were applied (see Figure 18(a)). However, both LVDT were connected to data logger device by specific cables. In terms

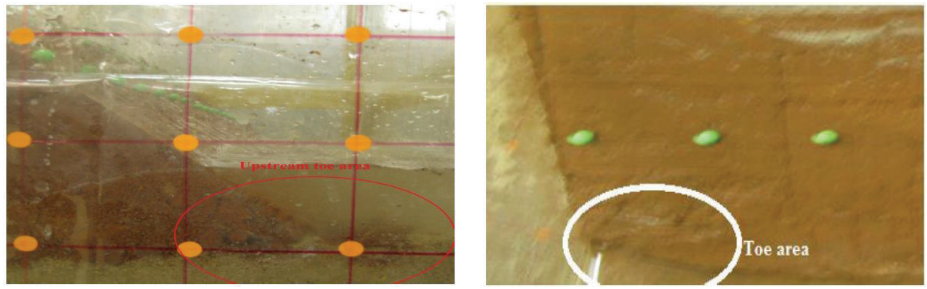

(a) (b)

Figure 22: Damage in the third model (Model C).

of compaction soil for each layer, the steel roller used was selected by trial error method. Wood molding with respect to control slope via network index was used. In order to avoid absorption of soil water content, both the described molds were just soaked by water before use. For tank purpose, small scale models were filled up by water with very slow rate.

After vibration equal to two minutes for all models, the vertical displacement for both slopes such as upstream and downstream were printed. With respect to use of Excel program, Figure 19 shows the distribution of vertical displacement in both edges in the middle of the crest and relative displacement in all models. It was obvious that distribution of the vertical displacement indicated a same trend for both models such as A and E. In both models, displacement values were negative during the vibration. It means that both of them were in uplift condition. In this figure also, maximum and minimum peak of the relative displacement, respectively, occurred in Models B and C with 2.13 mm and 0.06 mm. It is also worth noting that this value was at convergence position for Models A and E with 0.24 mm and 0.25 mm, respectively.

In terms of damage location in models, Figure 20 shows the damage in Model A which occurred at upstream and downstream. The level of damage was greater in upstream. It was very sensible occurrence in case of hydrodynamic pressure along the vibration. Also in this figure, the maximum longitudes cracks (see line C) were observed near to the middle of dam at the crest. For damage at downstream, the transverse cracks significantly occurred in dam toe.

Figure 21 shows Model B that was damaged after vibration. It can be observed that dam was significantly damaged in some locations such as crest and surfaces. Body cracks and failure process dramatically occurred in both areas near to abutments. Also in this figure, one transverse crack in the middle of the crest was seen (see Figure 20(c)). This damage was significantly repeated at upstream in Model C, but it was placed in dam toe, and it can be seen in Figure 22. In addition, Model D was damaged in three places such as both abutments and the middle of the upstream. Figure 23 shows Model D that was damaged in toe. Briefly, all four models were damaged, as discussed previously. On the other hand, a successful way in order to remove damage was obtained in Model E, as shown in Figure 24. Figure 24 shows that model

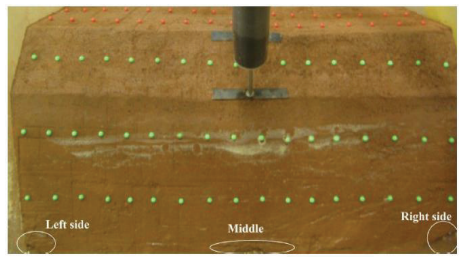

Figure 23: Damage in the fourth model (Model D).

was safe after vibration without any damage. In this figure, the reinforced blanket layer using IDL material was indicated by red circles between dam and foundation. In addition, it was very important to note that both surfaces were safe and dam was stable under severe seismic loading like resonance motion. In fact, a good absorption of energy with respect to increase of damping was found by using IDL. In case of using this technique, displacement in both edges of the crest with negative value indicated the uplift situation. Moreover, relative displacement was like the first model. Therefore, dam behavior before and after reinforcement was similar for both distributions of displacement. Nevertheless, Model E was successful to remove damage with respect to high level of damping in blanket layer. In fact, this model shows the excellent performance in earth dams when the blanket layer was expanded below tank.

Finally, blanket layer using isolator damper layer (IDL) below dam and tank is a good recommendation for earth dams in seismic zone when reinforced thickness is one-fourth of dam height. As recommended, optimization of thickness in this method is the next study.

6. Conclusion

In this study, the earth dam performance under severe seismic motion such as resonance was evaluated by using blanket layer (IDL). With respect to soil mechanic test, the optimum mixture for IDL was designed. IDL powder was made by using some materials. Main material was a local soil (laterite) with 90%, and additives such as TDA

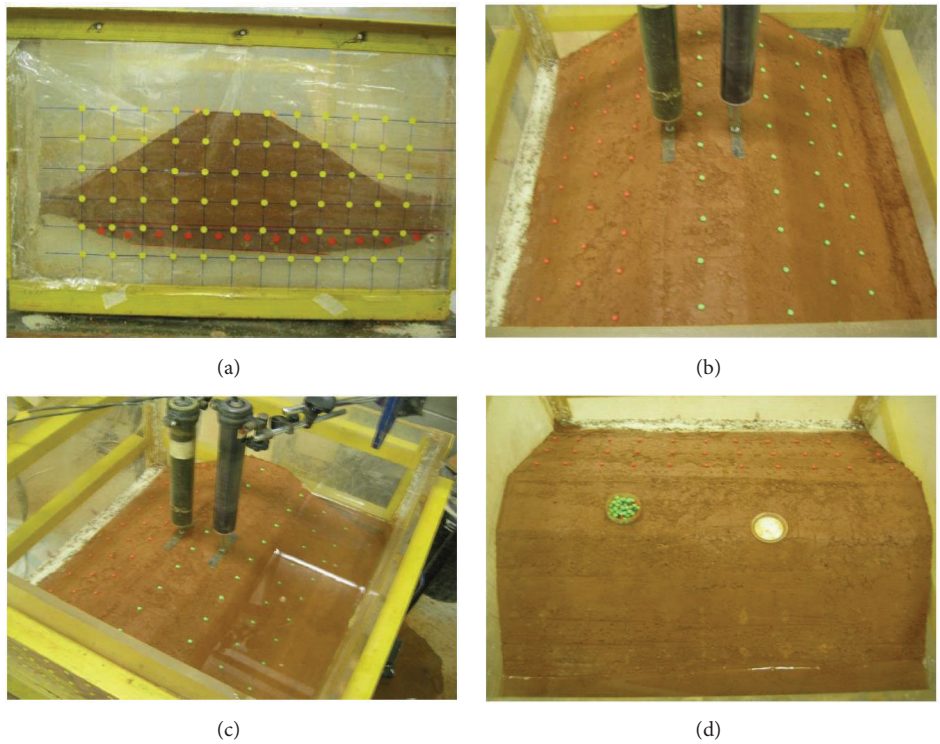

Figure 24: Dam stabilization in the fifth model (Model E).

(tire derived aggregate with 7%) and MS (microsilica) with 3% were used. This material was utilized to reinforce dam in small scale physical modeling. According to numerical analysis, the dominant frequency (0.2298 Hz) in order to have maximum effect for modeling vibration was computed. By using this frequency for physical modeling, the damage location and distribution of vertical displacement at both edges of the crest in the middle of small dams for five small model with scale 1/100 were discussed. As results, the best performance in order to remove damages was obviously observed in Model E while other models were dramatically damaged in some locations such as upstream, downstream, and crest. In addition, the thickness of blanket layer in this model was one-fourth of dam height. Finally, this model is a novel method to reinforce dam under strong earthquake like resonance phenomena recommended for earth dam design in seismic zone.

Conflict of Interests

The authors declare that there is no conflict of interests regarding the publication of this paper.

Acknowledgment

This study is made possible by the support of the International Doctorate Fellowship of Universiti Teknologi, Malaysia, and it is very much appreciated.

References

[1] M. Zeghal and A. M. Abdel-Ghaffar, "Analysis of behavior of earth dam using strong-motion earthquakes records," *Journal of Geotechnical Engineering*, vol. 118, no. 2, pp. 266–277, 1992.

[2] V. Gikas and M. Sakellariou, "Settlement analysis of the Mornos earth dam (Greece): evidence from numerical modeling and geodetic monitoring," *Engineering Structures*, vol. 30, no. 11, pp. 3074–3081, 2008.

[3] R. Verdugo, N. Sitar, J. D. Frost et al., "Seismic performance of earth structures during the February 2010 Maule, Chile, earthquake: dams, levees, tailings dams, and retaining walls," *Earthquake Spectra*, vol. 28, no. 1, pp. S75–S96, 2012.

[4] Y. Parish and F. N. Abadi, "Dynamic behaviour of earth dams for variation of earth material stiffness," *Proceedings of World Academy of Science: Engineering and Technology*, vol. 50, pp. 606–611, 2009.

[5] T. G. Berhe, X. T. Wang, and W. Wu, "Numerical investigation into the arrangement of clay core on the seismic performance of earth dams," in *Proceedings of the GeoShanghai International Conference on Soil Dynamics and Earthquake Engineering*, pp. 131–138, ASCE, June 2010.

[6] Z. F. Xia, G. L. Ye, J. H. Wang, B. Ye, and F. Zhang, "Fully coupled numerical analysis of repeated shake-consolidation process of earth embankment on liquefiable foundation," *Soil Dynamics and Earthquake Engineering*, vol. 30, no. 11, pp. 1309–1318, 2010.

[7] X. J. Kong, Y. Zhou, B. Xu, and D. G. Zou, "Analysis on seismic failure mechanism of Zipingpu dam and several reflections of aseismic design for high rock-fill dam," in *Proceedings of the Earth and Space*, pp. 3177–3189, March 2010.

[8] A. Bayraktar, M. E. Kartal, and S. Adanur, "The effect of concrete slabrockfill interface behavior on the earthquake performance of a CFR dam," *International Journal of Non-Linear Mechanics*, vol. 46, no. 1, pp. 35–46, 2011.

[9] R. P. Piao, A. H. Rippe, B. Myers, and K. W. Lane, "Earth dam liquefaction and deformation analysis using numerical modeling," in *Proceedings of the GeoCongress*, pp. 1–6, March 2006.

[10] A. W. Elgamal, "Three-dimensional seismic analysis of la villita dam," *Journal of Geotechnical Engineering*, vol. 118, no. 12, pp. 1937–1958, 1992.

[11] B. Gordan and B. A. Azlan, "Effect of material properties in CFRD tailing-embankment bridge during a strong earthquake," *Caspian Journal of Applied Sciences Research*, vol. 2, no. 11, pp. 61–72, 2013.

[12] A. Papalou and J. Bielak, "Seismic elastic response of Earth dams with canyon interaction," *Journal of Geotechnical and Geoenvironmental Engineering*, vol. 127, no. 5, pp. 446–453, 2001.

[13] Y. Yu, L. Xie, and B. Zhang, "Stability of earth-rockfill dams: influence of geometry on the three-dimensional effect," *Computers and Geotechnics*, vol. 32, no. 5, pp. 326–339, 2005.

[14] L. H. Mejia and H. B. Seed, "Comparison of 2-D and 3-D dynamic analyses of earth dams," *Journal of Geotechnical Engineering*, vol. 109, no. 11, pp. 1383–1398, 1983.

[15] J. L. Borges, "Three-dimensional analysis of embankments on soft soils incorporating vertical drains by finite element method," *Computers and Geotechnics*, vol. 31, no. 8, pp. 665–676, 2004.

[16] A. Yildiz, "Numerical analyses of embankments on PVD improved soft clays," *Advances in Engineering Software*, vol. 40, no. 10, pp. 1047–1055, 2009.

[17] B. Le Hello and P. Villard, "Embankments reinforced by piles and geosynthetics-Numerical and experimental studies dealing with the transfer of load on the soil embankment," *Engineering Geology*, vol. 106, no. 1-2, pp. 78–91, 2009.

[18] S. W. Abusharar, J. J. Zheng, B. G. Chen, and J. H. Yin, "A simplified method for analysis of a piled embankment reinforced with geosynthetics," *Geotextiles and Geomembranes*, vol. 27, no. 1, pp. 39–52, 2009.

[19] R. Noorzad and M. Omidvar, "Seismic displacement analysis of embankment dams with reinforced cohesive shell," *Soil Dynamics and Earthquake Engineering*, vol. 30, no. 11, pp. 1149–1157, 2010.

[20] T. Matsumaru, K. Watanabe, and J. Isono, "Application of cement-mixed gravel reinforced by ground for soft ground improvement," in *Proceedings of the 4th Asian Regional Conference on Geosynthetics*, pp. 380–385, Shanghai, China, June 2008.

[21] Namdar and A. A. K. Pelko, "Seismic evaluation of embankment shaking table test and finite element method," *The Pacific Journal of Science and Technology*, vol. 11, no. 2, 2010, http://www.akamaiuniversity.us/PJST.

[22] L. Wang, G. Zhang, and J. Zhang, "Centrifuge model tests of geotextile-reinforced soil embankments during an earthquake," *Geotextiles and Geomembranes*, vol. 29, no. 3, pp. 222–232, 2011.

[23] H. B. Seed, R. T. Wong, I. M. Idriss, and K. Tokimatsu, "Moduli and damping factors for dynamic analyses of cohesionless soils," *Journal of Geotechnical Engineering*, vol. 112, no. 11, pp. 1016–1032, 1986.

[24] B. M. Das, *Advanced Soil Mechanics*, CRC Press, New York, NY, USA, 2013.

[25] M. J. Griffin, *Handbook of Human Vibration*, Academic Press, New York, NY, USA, 2012.

[26] J. Garnier, C. Gaudin, S. M. Springman, P. J. Culligan, D. J. Goodings, and D. Konig, "Catalogue of scaling laws and similitude questions in geotechnical centrifuge modelling," *International Journal of Physical Modelling in Geotechnics*, vol. 7, no. 3, pp. 1–23, 2007.

[27] A. Fluent, *12.0 User's Guide*, User Inputs for Porous Media, 2009.